JACS
JOURNAL OF THE AMERICAN CHEMICAL SOCIETY
pubs.acs.org/JACS
Article

# Impact of Molecular Design on Degradation Lifetimes of Degradable Imine-Based Semiconducting Polymers

Jerika A. Chiong, Yu Zheng, Song Zhang, Guorong Ma, Yilei Wu, Gradie Ngaruka, Yangju Lin, Xiaodan Gu, and Zhenan Bao*

Cite This: https://doi.org/10.1021/jacs.1c12845
Read Online
ACCESS | Metrics & More | Article Recommendations | Supporting Information

**ABSTRACT:** Transient electronics are a rapidly emerging field due to their potential applications in the environment and human health. Recently, a few studies have incorporated acid-labile imine bonds into polymer semiconductors to impart transience; however, understanding of the structure−degradation property relationships of these polymers is limited. In this study, we systematically design and characterize a series of fully degradable diketopyrrolopyrrole-based polymers with engineered sidechains to investigate the impact of several molecular design parameters on the degradation lifetimes of these polymers. By monitoring degradation kinetics via ultraviolet−visible spectroscopy, we reveal that polymer degradation in solution is aggregation-dependent based on the branching point and $M_n$, with accelerated degradation rates facilitated by decreasing aggregation. Additionally, increasing the hydrophilicity of the polymers promotes water diffusion and therefore acid hydrolysis of the imine bonds along the polymer backbone. The aggregation properties and degradation lifetimes of these polymers rely heavily on solvent, with polymers in chlorobenzene taking six times as long to degrade as in chloroform. We develop a new method for quantifying the degradation of polymers in the thin film and observe that similar factors and considerations (e.g., interchain order, crystallite size, and hydrophilicity) used for designing high-performance semiconductors impact the degradation of imine-based polymer semiconductors. We found that terpolymerization serves as an attractive approach for achieving degradable semiconductors with both good charge transport and tuned degradation properties. This study provides crucial principles for the molecular design of degradable semiconducting polymers, and we anticipate that these findings will expedite progress toward transient electronics with controlled lifetimes.

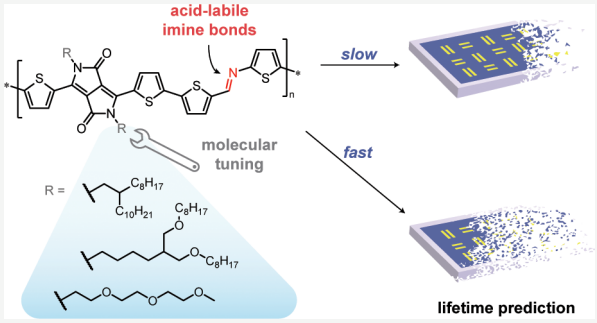


## 1. INTRODUCTION

With the pressing need for a sustainable future in the technology-driven 21st century, transient electronics have garnered much interest for their potential ability to degrade after a certain, designated lifetime or upon applied external stimuli.[1−3] Such degradable electronics would allow for (i) the reduction of our rapidly growing electronic waste, (ii) the elimination of secondary removal surgeries for implantable devices, and (iii) transience in the environment in which remote, widespread sensors can be deployed without necessity of recollection.[4−9] Recent advances in the field of transient electronics employ a biodegradable arterial-pulse sensor for blood flow monitoring,[10] an implantable triboelectric nanogenerator for in vivo energy harvesting,[11] and a multifunctional sensor for noninvasive personal care diagnostics.[12]

Of the currently reported transient devices, most consist of degradable encapsulant, substrate, and dielectric materials with nondegradable electronically active components (i.e., semiconductors and conductors).[13] Synthetic polymers serve as an attractive platform for the development of degradable semiconductors due to their ability to be rationally tuned by molecular design for exploration of desired morphological, electronic, and degradation properties. Additionally, these polymers have the potential for integration of skin-inspired functionalities (e.g., stretchability, conformability, self-healing, and adhesivity).[14−19] However, owing to the limited number of degradable bonds that maintain conjugation along the polymer backbone for high-performance devices, there are only a few reports of degradable semiconducting polymers.[13,20−24] As a result, the degradation behavior of semiconducting polymers in relation to molecular design has not been properly studied. As several works on tuning the degradation rate of nonconjugated polymeric materials have been reported[25−28] and various methods of improving semiconductor charge transport properties have been investigated, such as through backbone or

Received: December 17, 2021





https://doi.org/10.1021/jacs.1c12845
J. Am. Chem. Soc. XXXX, XXX, XXX−XXX

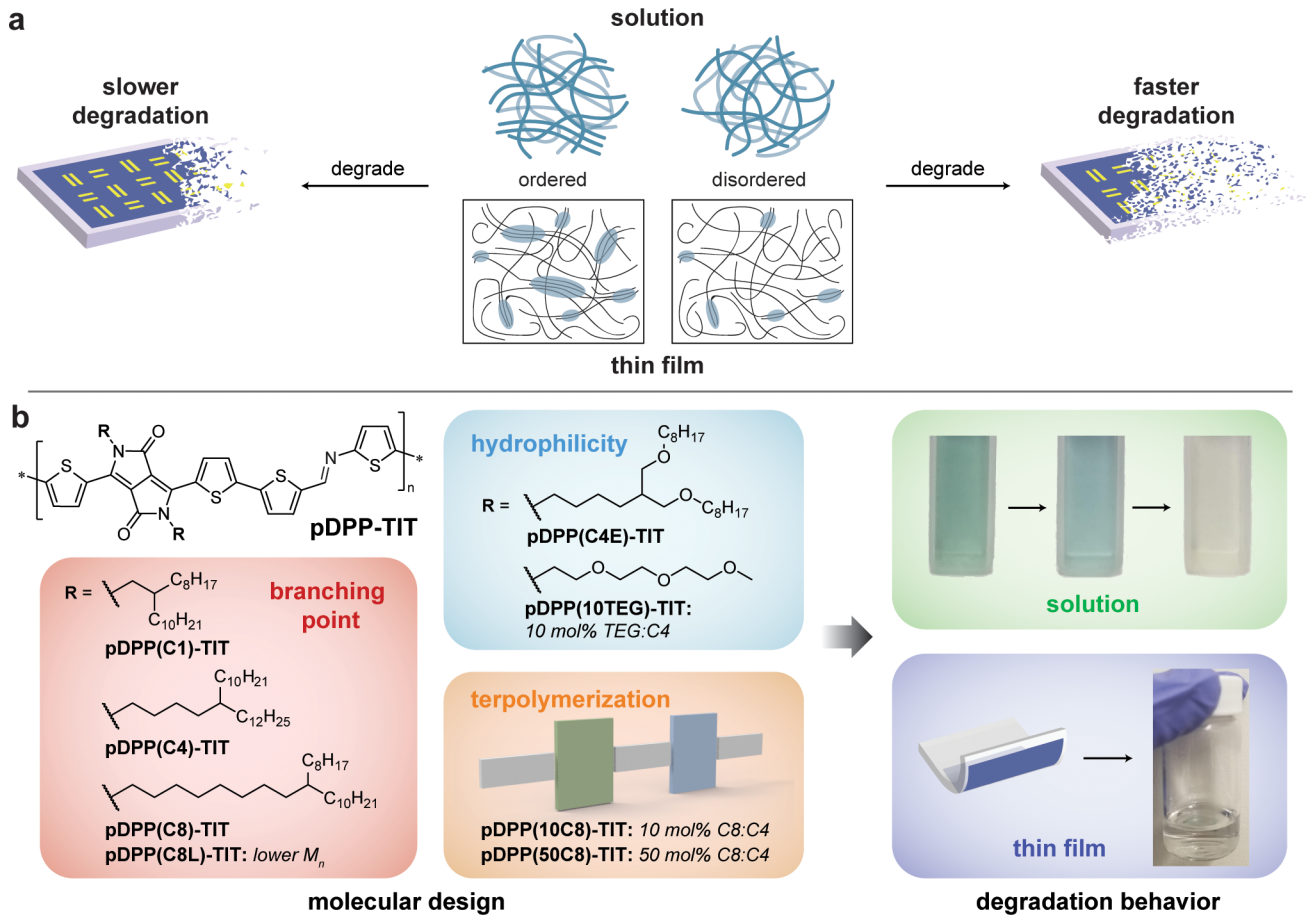


**Figure 1.** General schematic and molecular design of this study. (a) Understanding of solution and thin film structure−property relationships of degradable polymer semiconductors will enable the potential to achieve transient electronics with controlled degradation lifetimes. (b) Molecular design parameters and polymers explored for investigation of solution and thin film degradation behavior.

sidechain engineering,[29−37] similar molecular engineering approaches should also be possible for the tuning of semiconducting polymer degradation behavior. Such understanding of how polymer design and the corresponding assembly in condensed states affect degradation behavior will enable the realization of transient electronics with controlled, targeted lifespans (Figure 1a).

Our previous studies on degradable semiconducting polymers featured acid-labile imine bonds to impart transience, in which imine hydrolysis along the polymer backbone led to cleavage of the polymer chain.[20,21] We described a modular approach to prepare degradable imine-based semiconducting polymers with an electronic performance comparable to their nondegradable counterparts by Stille cross-couplings. This facile method of polymerization enabled the preparation of both *p*-type and *n*-type imine-based donor−acceptor (D−A) conjugated polymers, expanding the field of the existing degradable semiconductors. While prior studies confirmed the degradation of these semiconducting polymers into oligomers and monomers, there was limited control in the polymer degradation timescales and lifespans of the corresponding transient devices. We observed that the *n*-type naphthalene diimide-based semiconductor degraded much faster than the *p*-type diketopyrrolopyrrole (DPP)-based one, which was hypothetically ascribed to the increased aggregation of the latter; however, the study of the aggregation behavior of these degradable semiconducting polymers is yet to be conducted. Comparisons of the degradation behavior across different imine-based semiconducting polymers with respect to their morphological and electronic properties have also not been closely studied.

Herein, we use Stille cross-couplings to prepare imine-based semiconductors with tuned polymer structures for the systematic exploration of structure−property relationships of degradable semiconducting polymers. These D−A copolymers were synthesized from dibromo-functionalized, thiophene-flanked DPP and ditin-functionalized thiophene-imine-thiophene (TIT) monomers to produce degradable pDPP-TIT. Inspired by previous reports of sidechain engineering of semiconducting polymers in which structural modification of chain length, branching point, asymmetry, and hydrophilicity substantially impacts molecular packing and resulting charge carrier properties, we design a series of DPP-based monomers with five different sidechains to rationally examine their effect on degradation behavior and electronic performance (Figure 1b). It was demonstrated that moving the branching point of conventional branched alkyl chains away from the polymer backbone reduced $\pi-\pi$ stacking distances in polymer thin films and had a significant improvement in charge carrier mobilities.[31−33] To examine the influence of the branching point distance on degradation time, we introduce three asymmetric branched alkyl sidechains with C1, C4, and C8 spacers onto the DPP core, where C*n* refers to the number of carbons between the ketopyrrole nitrogen and the branching


https://doi.org/10.1021/jacs.1c12845
J. Am. Chem. Soc. XXXX, XXX, XXX−XXX

point. Additionally, oligoether sidechains have garnered interest for optoelectronic applications due to their hydrophilicity, polarity, and flexibility.[38] As the degradation of the imine-based polymers occurs through acid hydrolysis, tuning sidechain hydrophilicity has the potential to further influence the imine bonds' degree of interaction with water. Therefore, we aim to investigate the effect of hydrophilic sidechains by employing triethylene glycol (TEG) and a modified, branched alkyl C4 spacer sidechain with ether functionalities (C4E). Lastly, terpolymerization is employed as a method to further tune degradable semiconducting polymer properties using the same synthesized monomer building blocks.

To examine the influence of sidechain modification on the semiconducting polymers' aggregation properties and degradation behavior, we characterized the polymers by gel permeation chromatography (GPC), ultraviolet−visible (UV−vis) absorption spectroscopy, and grazing-incidence X-ray diffraction (GIXD). The electronic performance of these polymers was measured by fabricating thin-film field-effect transistors (FETs). To quantitatively probe degradation behavior, we monitored and compared the different polymers' degradation in solution by UV−vis and observed that aggregation and hydrophilicity indeed affected degradation times. Moreover, we developed a new technique of floating polydimethylsiloxane (PDMS) substrates on acidic solution to measure the degradation of polymer thin films and discovered that similar parameters that dictate electronic performance of semicrystalline polymer semiconductors also influence their degradation kinetics. Our results suggest that introducing hydrophilic functionalities through terpolymerization serves as a promising design approach for accelerating degradation of imine-based semiconductors while maintaining high charge carrier mobility. The rational tuning and characterization of degradable imine-based polymer semiconductors described herein further the understanding of molecular design principles for transient electronics.

## 2. RESULTS AND DISCUSSION

**2.1. Synthesis of Degradable Semiconducting Polymers.** The synthetic route for dibromo-functionalized DPP-based monomers with rationally designed sidechains is outlined in Figure S1 using procedures analogous to those reported in literature.[39−42] The degradable, ditin-functionalized TIT monomeric unit (Sn-TIT-Sn) was synthesized in two steps from commercial starting materials as previously described.[22] The detailed synthetic procedures and characterizations are described in Figures S2−S9.

The imine-based D−A semiconducting polymers were synthesized via Stille condensation polymerization using tris(dibenzylideneacetone)dipalladium(0) ($Pd_2(dba)_3$) and tris(*o*-tolyl)phosphine ($P(o\text{-tol})_3$) as catalysts (Figures S10−S17). pDPP-TIT bipolymers (composed of two different monomers) were synthesized using C1, C4, C8, and C4E sidechains on the DPP core. Due to the insolubility of the pDPP-TIT polymer when functionalized with the TEG sidechain in organic solvents used for degradation studies and device processing, the TEG chain was incorporated using a 9:1 C4:TEG molar ratio to produce a pDPP(10TEG)-TIT terpolymer (composed of three different monomers) (Figure S15). Additional terpolymers were synthesized to determine whether the effect of the TEG chain on degradation and electronic performance was due to structure and hydrophilicity or reduced regioregularity from terpolymerization.[16,43] pDPP-(10C8)-TIT and pDPP(50C8)-TIT were polymerized using a 9:1 and 1:1 C4:C8 ratio, respectively (Figures S16 and 17).

The number-average molecular weight ($M_n$), dispersity ($Đ$), and number-average degree of polymerization ($DP_n$) were determined by high-temperature GPC (HT-GPC) using trichlorobenzene as the solvent at 180 °C and are summarized in Table 1. Similar to the previous study on pDPP(C4)-TIT,[22] t1

**Table 1. HT-GPC Characterization**

| polymer | $M_n$ (kg/mol) | $Đ$ | $DP_n$ |
|---|---|---|---|
| pDPP(C1)-TIT | 23.8 | 3.5 | 23 |
| pDPP(C4)-TIT | 21.4 | 2.8 | 17 |
| pDPP(C8)-TIT | 33.2 | 3.2 | 27 |
| pDPP(C8L)-TIT | 15.9 | 3.6 | 13 |
| pDPP(C4E)-TIT | 20.1 | 3.3 | 17 |
| pDPP(10TEG)-TIT | 32.1 | 2.7 | 27 |
| pDPP(10C8)-TIT | 33.3 | 2.9 | 27 |
| pDPP(50C8)-TIT | 33.1 | 2.6 | 27 |

we found that pDPP-TIT polymers with $M_n$ above 35 kg/mol were largely insoluble in common organic solvents (e.g., chloroform, toluene, and chlorobenzene) used for degradation studies and thin film preparation. Therefore, $M_n$ values were targeted to be around 20−35 kg/mol for proper comparison among degradable polymers, with the exception of an additional lower $M_n$ C8 sidechain polymer to examine the effect of molecular weight on degradation behavior. The lower $M_n$ C8 sidechain polymer will be abbreviated C8L, and all polymers will be addressed by their sidechain structure.

**2.2. Optical and Morphological Characterization.** We first characterized the optical and morphological properties of semiconducting polymers both in solution and as a thin film and examined any differences among the various sidechains studied. UV−vis was performed to evaluate the effects of the sidechain structure on the optical and aggregation properties of the degradable polymer. Similar to other DPP-based polymers,[22,43,44] the pDPP-TIT polymers showed two vibronic bands between 650 and 900 nm, labeled as 0−1 and 0−0 peaks (Figure 2). The full absorption spectra of all polymers are shown in Figures S18−S22. Previous studies attributed the lower energy 0−0 peak ($\lambda_{0-0}$) to interchain electronic interactions or polymer aggregation.[44,45] In dilute chlorobenzene solution (0.01 mg/mL), the effect of branching point was unclear, as both positioning the branching point closer to and further away from the backbone as in the C1 and C8 polymers displayed an increased $\lambda_{0-0}$ intensity compared to C4 (Figure 2a). Contrary to previous studies on the branching point of D−A-conjugated polymers,[32,33] the C1 polymer was both red-shifted and had a stronger $\lambda_{0-0}$ intensity relative to C4 despite their similar $M_n$. Although the hydrophilic C4E polymer had a similar $\lambda_{0-0}$ intensity relative to the C4 polymer, the vibronic bands were broadened (Figure 2b). All terpolymers displayed a higher $\lambda_{0-0}$ relative to C4; however, the increase in $\lambda_{0-0}$ intensity corresponded more to the higher $M_n$ (>30 kg/mol) of the polymers than any structural differences, as observed upon comparison of C8 and C8L polymers. Similar trends were observed in chloroform and toluene solutions (Figures S19−S20). However, when the polymers were cast as thin films from chlorobenzene solution and annealed (200 °C for 30 min), the C1 polymer showed a weaker $\lambda_{0-0}$ compared to C4 and C8 (Figure 2c), indicating that C1 has a weaker tendency to form interchain aggregates in the thin film. C4E


https://doi.org/10.1021/jacs.1c12845
J. Am. Chem. Soc. XXXX, XXX, XXX−XXX

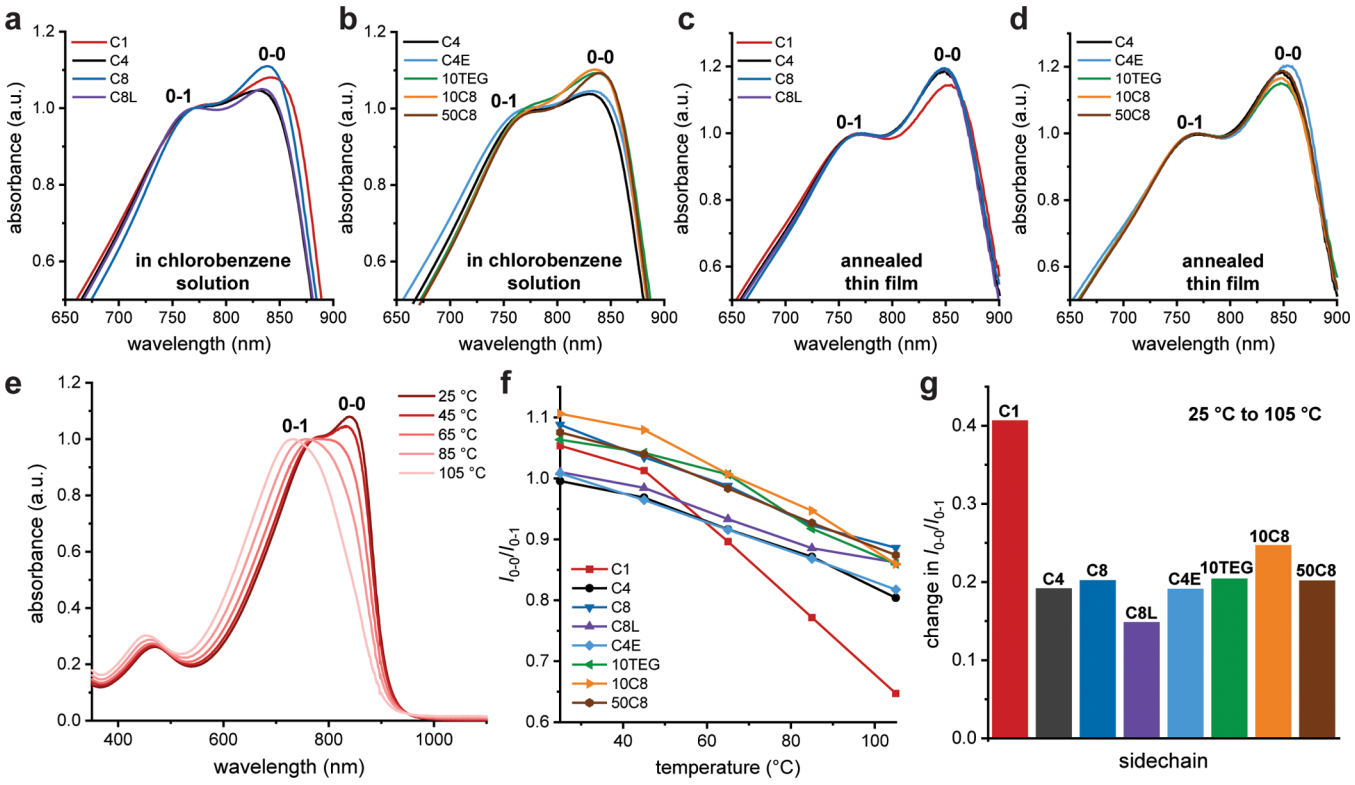


**Figure 2.** Optical property characterization. Normalized UV−vis absorption spectra of degradable pDPP-TIT polymers in (a,b) chlorobenzene solution (0.01 mg/mL) at 25 °C and (c,d) annealed thin films spin-coated from chlorobenzene. (e) Representative UV−vis spectra for pDPP(C1)-TIT in chlorobenzene solution at 25−105 °C, with 20 °C intervals. (f) Temperature dependence of interchain aggregation among polymers based on the 0−0 absorption peak. (g) Total change in interchain aggregation from 25 to 105 °C.

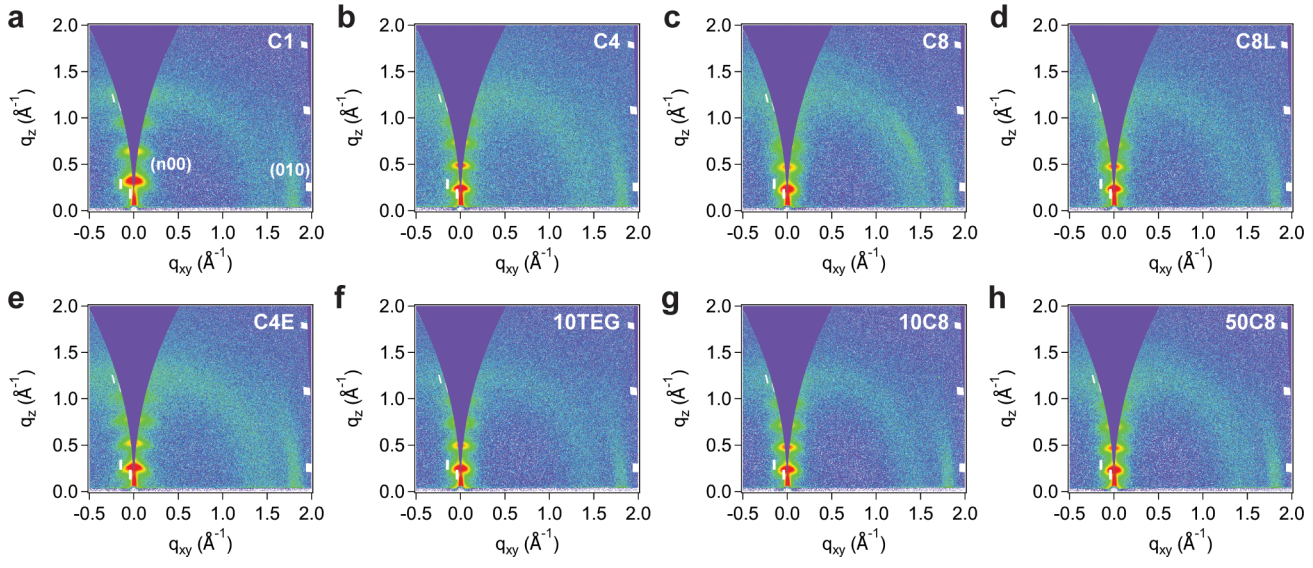


**Figure 3.** Morphology characterization. GIXD patterns of the spin-coated polymer thin films for (a) C1, (b) C4, (c) C8, (d) C8L, (e) C4E, (f) 10TEG, (g) 10C8, and (h) 50C8.

had the strongest $\lambda_{0-0}$ in the thin film, but the lower energy absorption band was slightly broadened in both solution and thin film (Figure 2d). When examining the terpolymers, we hypothesize that 10TEG showed a weaker $\lambda_{0-0}$ compared to the reference C4 polymer due to the regioirregularity introduced by terpolymerization of C4 and TEG, which are very structurally different. Additionally, 50C8 displayed a slightly higher $\lambda_{0-0}$ relative to 10C8, which can be potentially attributed to a larger ratio of C8 sidechains or a 1:1 C4:C8 ratio being more regioregular than 9:1.

To further investigate the solution-phase aggregation properties of the polymers, variable-temperature UV−vis spectra were measured for all polymers from 25 to 105 °C, with 20 °C intervals (Figure 2e and Figure S23). With the increasing temperature, the polymers exhibited temperature-dependent disaggregation, as shown by the decreasing $\lambda_{0-0}$


https://doi.org/10.1021/jacs.1c12845
J. Am. Chem. Soc. XXXX, XXX, XXX−XXX

peak intensity. Simple deconvolution analysis was performed for the 0−1 and 0−0 peaks, and the ratios of these intensities ($I_{0-0}/I_{0-1}$) were calculated, with larger values indicating more aggregation among polymer chains. All polymers displayed a similar aggregate stability with respect to heating except for C1 (Figure 2f,g). This observation that the C1 polymer more readily disaggregates with temperature suggests that its aggregates at room temperature are less stable (e.g., weaker interactions or smaller aggregates) compared to the other polymers.

The highest occupied molecular orbital (HOMO) energy levels were obtained by photoelectronic spectroscopy in air (PESA). The optical band gap, taken from the onset of absorption in UV−vis of annealed thin films, was subtracted from the HOMO to estimate the lowest unoccupied molecular orbital energy level. The results are summarized in Table S1. The HOMO energies and optical band gaps for all polymers were similar, suggesting that altering sidechains on the pDPP-TIT backbone had minimal effect on electronic structure.

To characterize the polymers' thin film morphology and crystallite packing in thin film, we performed atomic force microscopy (AFM) and GIXD measurements. AFM height and phase images are shown in Figure S24. All polymers had root mean square surface roughness values below 1.3 nm, indicating smooth films. 2D GIXD patterns for all polymers cast from chlorobenzene onto octadecyltrimethoxysilane (OTS)-modified Si wafers and annealed at 200 °C for 30 min are shown in Figure 3. Plane spacings, full width half maxima (fwhm), and crystallite coherence length (CCL) are shown in Table 2. The corresponding in-plane and out-of-plane scattering profiles are shown in Figure S25. All pDPP-TIT polymers exhibited a predominantly edge-on orientation, with out-of-plane ($n$00) lamellar stacking peaks along the $q_z$ direction and one in-plane (010) $\pi-\pi$ stacking peak in the $q_{xy}$ direction. The scattering along the $q_{xy}$ direction at 1.4 Å$^{-1}$ in all 2D patterns is attributed to the OTS surface modification. The lamellar spacing values result from the overall length of the sidechains, with the C1 spacer sidechain being shorter than both the C4 and C8 spacers. The C4E sidechain also showed smaller lamella spacing than the reference C4 sidechain due to it being shorter than C4 on one of the sidechain branches as well as the increased flexibility of the oxygen atoms compared to rigid alkyl chains.[38] C1 had a very slightly larger $\pi-\pi$ stacking distance than those of the other bipolymers, which follows the trend observed in previous studies that demonstrate that having the branching point closer to the backbone inhibits close $\pi-\pi$ stacking in the thin film.[32] However, it must be noted that the difference in $\pi-\pi$ spacing distances of pDPP-TIT polymers (~0.02 Å) between one and at least four carbon spacers was drastically smaller than those observed previously for isoindigo-based polymers (~0.2 Å).[31,32] This result explains the lack of significant difference in aggregation behavior and electronic structure measured by UV−vis and PESA among C1, C4, and C8 polymers. C1 and C4E showed a larger $\pi-\pi$ fwhm and smaller CCL based on the (010) peak than all other bipolymers, corresponding to lower finite crystallite grain size or greater cumulative lattice disorder along the $\pi-\pi$ stacking direction. The terpolymers (10TEG, 10C8, and 50C8) displayed a similar reduced CCL compared to C4, indicating a more disordered morphology, which is supported by our work that demonstrated terpolymerization resulted in decreased large crystalline domains.[16] We did not observe a correlation between thin film UV−vis $\lambda_{0-0}$ intensity of the terpolymers and GIXD measurements likely because GIXD probes only longer-range crystalline domains while UV−vis absorbance comes from a combination of both longer- and shorter-range aggregates.

**Table 2. Relevant Crystallographic Parameters from GIXD**

| sidechain | lamellar spacing (Å)[a] | lamellar fwhm (Å$^{-1}$)[b] | $\pi-\pi$ spacing (Å)[c] | $\pi-\pi$ fwhm (Å$^{-1}$) | CCL (Å)[d] |
|---|---|---|---|---|---|
| C1 | 19.3 | 0.04 | 3.46 | 0.18 | 8.1 |
| C4 | 25.5 | 0.03 | 3.44 | 0.13 | 10.9 |
| C8 | 26.6 | 0.04 | 3.42 | 0.14 | 10.2 |
| C8L | 26.2 | 0.03 | 3.43 | 0.14 | 10.5 |
| C4E | 23.8 | 0.03 | 3.44 | 0.15 | 9.4 |
| 10TEG | 25.1 | 0.03 | 3.45 | 0.15 | 9.4 |
| 10C8 | 26.0 | 0.03 | 3.45 | 0.14 | 9.9 |
| 50C8 | 26.7 | 0.03 | 3.43 | 0.15 | 9.2 |

[a]Extracted from fitting the (100) diffraction peak. [b]fwhm represents the full width at half-maximum for the peak. [c]Extracted from fitting the (010) diffraction peak. [d]Calculated based on the $\pi-\pi$ stacking peak fwhm using the Scherrer equation. CCL = crystallite coherence length

**2.3. Electronic Performance of FETs.** We fabricated bottom-gate top-contact FETs to measure the charge carrier mobilities of the degradable polymer semiconductors using OTS-modified $SiO_2$ as the dielectric, highly doped Si as the gate, and Au as the source and drain electrodes. Detailed fabrication procedures are described in the Supporting Information. Representative transfer curves for the degradable imine-based semiconductors operated in both the saturation and linear regimes are shown in Figure 4 and Figure S26. Output curves for each polymer are depicted in Figure S27. The average mobilities and performance metrics of the pDPP-TIT polymers with different sidechains are summarized in Figure 4c and Table S2. FETs exhibited dominant p-channel behavior under ambient conditions. First examining branching point, C4 and C8 showed average saturation hole mobilities ($\mu_{sat}$) of 0.65 and 0.56 cm$^2$/V·s, respectively. C1 displayed a reduced $\mu_{sat}$, which can be attributed to slightly weaker $\pi-\pi$ interchain interactions[32] and shorter-range order of the aggregates (from lower CCL) based on UV−vis and GIXD experiments, respectively. Comparing C8 and C8L polymers, higher $M_n$ values improved mobilities but to a lesser degree than moving the branching point away from the backbone. Additionally, C4E had a much lower $\mu_{sat}$ than other polymers, which we attribute to potential water traps or ionic impurities due to the hydrophilicity of the sidechain.[46] 10TEG also showed slightly reduced mobilities due to the slight hydrophilicity imparted by the 10 mol % TEG sidechains in the terpolymer. Lastly, the terpolymers generally displayed comparable mobilities to those of the bipolymers with their respective sidechains, as we hypothesize that they contain a comparable degree of short-range order with slightly decreased longer-range order along the $\pi-\pi$ stacking direction (indicated by their lower CCL).[16]

**2.4. Degradation Timescale Studies.** We used UV−vis to monitor the degradation of imine-based semiconducting polymers both in solution and thin film. As the imine bonds cleave, the polymers degrade into oligomers and eventually monomers, which have minimal absorption in the visible region. For solution degradation studies, trifluoroacetic acid (TFA) and water were added to a dilute polymer solution (0.8


https://doi.org/10.1021/jacs.1c12845
J. Am. Chem. Soc. XXXX, XXX, XXX−XXX

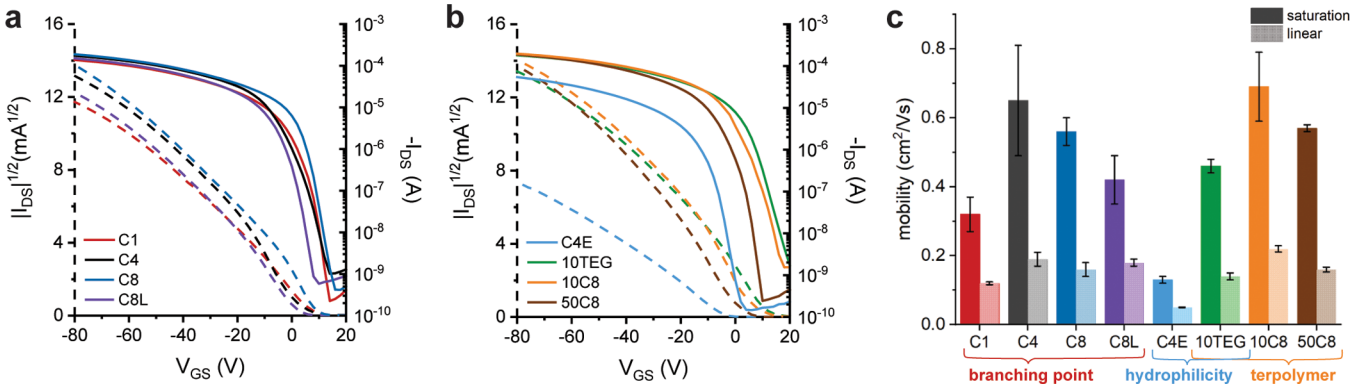


**Figure 4.** Electronic performance of FETs. (a,b) Representative saturation transfer curves for polymers ($V_{DS}$ = −80 V). The dashed lines correspond to the square root of the drain current. (c) Average charge carrier mobilities (extracted from the saturation and linear regimes) of the degradable semiconductor films.

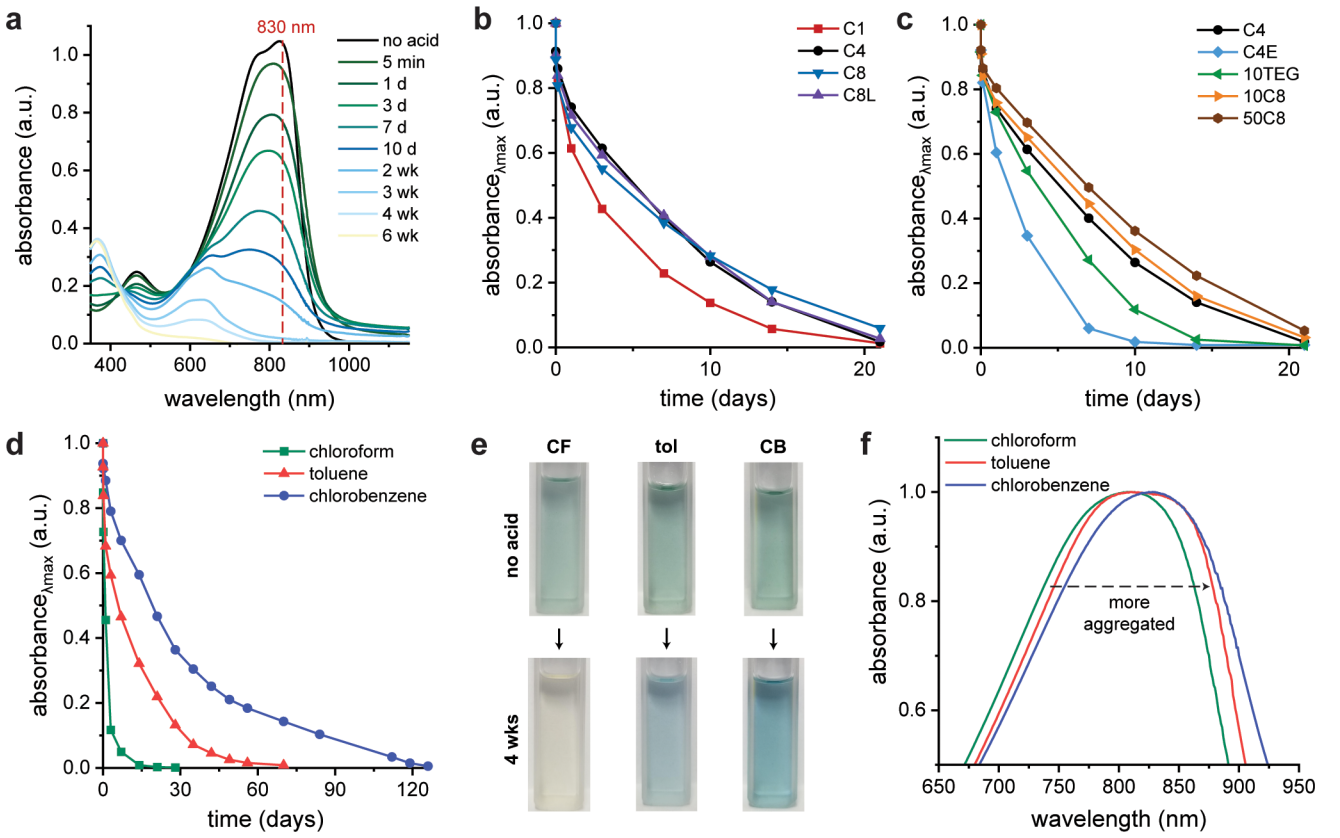


**Figure 5.** Solution degradation studies by UV−vis spectroscopy. (a) Representative UV−vis spectra for pDPP(C4)-TIT in chloroform solution (~0.01 mg/mL) monitored over time upon addition of acid and water. (b,c) UV−vis absorption intensities at 830 nm are plotted over time for degradation of all polymers in chloroform (normalized to time = 0). (d) Solvent dependence of solution degradation studies for pDPP(C4)-TIT in chloroform, toluene, and chlorobenzene (normalized to time = 0). (e) Photographs of original and degraded solutions for pDPP(C4)-TIT in different solvents after 4 weeks. (f) Normalized UV−vis spectra of pDPP(C4)-TIT in different solvents upon treatment of an equivalent amount of acid and water at 25 °C.

μM imine) in various organic solvents. Chloroform, toluene, and chlorobenzene, which are solvents that are typically used to dissolve D−A-conjugated polymers, were chosen for solution degradation studies. The degradation of the series of pDPP-TIT polymers in chloroform at room temperature with a 1000-fold molar excess of acid and water is shown in Figure 5a−c and Figure S28. As the polymers degraded, the lower energy absorption band, which corresponds to polymer interchain interactions, decreased and blue-shifted as the polymers decreased in conjugation length (Figure 5a). Additionally, the $\pi-\pi^*$ transition at 450−500 nm associated with intrachain charge delocalization diminished as the DPP units hydrolyzed and ring-opened, resulting in complete degradation of the pDPP-TIT polymers.[20,44,45] To quantify the degradation of the different polymers in solution, all spectra were normalized to the $\lambda_{0-1}$ of the original, undegraded polymer and the decrease in absorbance at the $\lambda_{max}$ (830 nm for chloroform solution), which was chosen as it indicated imine bond cleavage, was measured over time. We defined polymers as degraded when their absorbance intensity at $\lambda_{max}$


https://doi.org/10.1021/jacs.1c12845
J. Am. Chem. Soc. XXXX, XXX, XXX−XXX

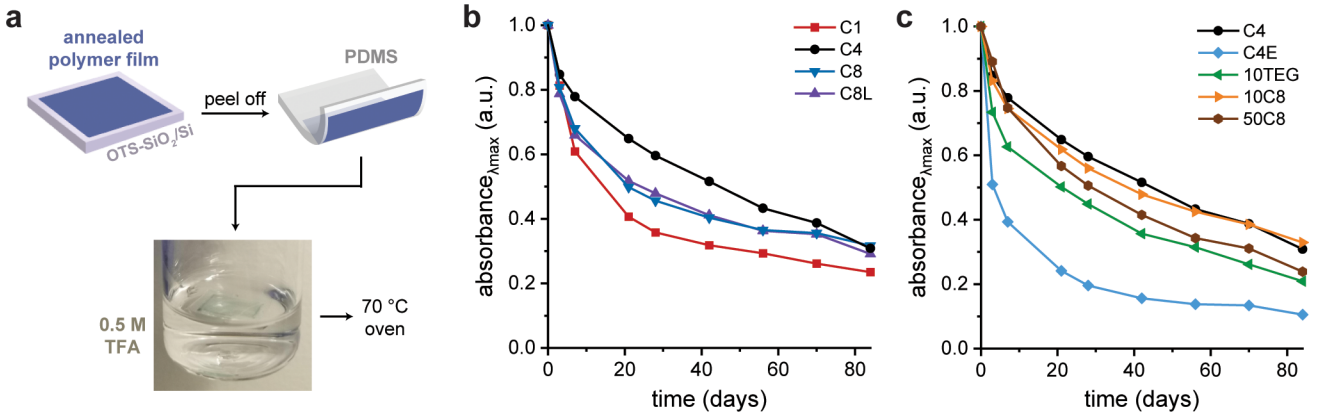


**Figure 6.** Thin film degradation studies by UV−vis spectroscopy. (a) Developed floating PDMS technique for measurement of polymer thin film degradation. (b,c) UV−vis absorption intensities at 850 nm are plotted over time for degradation of annealed polymer thin films (normalized to time = 0).

was ≤0.05 a.u. (i.e., the absorbance corresponding to polymer interchain aggregation was ≤5% of that of the original polymer). As observed in Figure 5b, the C1 sidechain degraded faster relative to C4 and C8 sidechains, suggesting that placing the branching point closer to the polymer backbone inhibits strong interchain aggregation. This observation agrees with our variable-temperature UV−vis experiments that displayed C1 readily disaggregated with the increase in temperature. Moving the branching point more than four carbons away, as in the C8 spacer, had minimal effect on degradation time. Additionally, sidechains with hydrophilic functionalities, C4E and 10TEG, degraded faster than all other polymers, with C4E degrading in half the amount of time as the representative C4 polymer without any oxygen units (Figure 5c). The slight hydrophilicity given by the incorporation of TEG at 10 mol % also caused this polymer to degrade at a shorter timescale than C4. The terpolymers (10C8 and 50C8) had degradation times that were similar to their C4 and C8 bipolymer counterparts, with a slightly slower degradation observed likely due to their higher $M_n$.

The aggregation-dependent degradation of these polymers in solution (dependent on branching point and $M_n$) was observed in both toluene and chlorobenzene solutions as well (Figures S29−S31). However, the effect of hydrophilicity was only observed in chloroform. We hypothesize that the hydrophilicity of C4E and 10TEG accelerated the degradation rates in chloroform solution due to the increased solubility of water in chloroform (0.056%) compared to aromatic solvents (0.033% in toluene and 0.04% in chlorobenzene).[47−50] Therefore, hydrophilicity of the polymers facilitated acid hydrolysis of imine bonds in solution but only when the solvent was able to effectively solubilize the water necessary for reaction. Interestingly, when an equivalent amount of acid and water were added to each of the polymer solutions in the three solvents, the degradation rate differed dramatically depending on the solvent (Figure 5d,e). While the C4 polymer degraded in less than 20 days in chloroform, the degradation in toluene took over three times as long. Additionally, the degradation in chlorobenzene was even slower, taking over six times as long as in chloroform. We conducted NMR degradation experiments of the TIT monomer to verify that acid hydrolysis of the imine bond was not solvent-dependent (Figure S32), and thus, the variation in degradation time was likely caused by aggregation or other factors. To rationalize the solvent dependence of the polymers' degradation, we examined the UV−vis spectra of pDPP(C4)-TIT across all three solutions right after adding equivalent amounts of TFA and water (Figure 5f and Figure S33). A redshift in the absorption spectra was observed for all polymer solutions upon addition of acid due to potential acid doping,[51−53] with the largest redshift seen in chlorobenzene solution. We hypothesize that the redshift corresponded to acid-induced aggregation, which resulted in the slowest degradation for polymers in chlorobenzene solution. Additionally, in the UV−vis spectra of the undegraded C4 polymer, the lower energy absorption band was well-overlapped for chloroform and toluene solutions, with toluene displaying a stronger $\lambda_{0-0}$ intensity and thus stronger interchain aggregation (Figure S33). Although the $\lambda_{0-0}$ intensity of chlorobenzene was weaker than that of toluene, the vibronic bands were redshifted altogether, suggesting a different type of aggregates formed in chlorobenzene. These observations were supported by diffusion ordered spectroscopy (DOSY) experiments, which showed that the hydrodynamic radius (aggregation size) of the C4 polymer was larger in chlorobenzene than in chloroform (Table S3). At the concentration used for DOSY experiments (10× degradation conditions), all polymers precipitated out of toluene solutions. Further studies on the solvent dependence of degradable, imine-based polymer semiconductors and their aggregation in solution will have to be conducted for conclusive attribution of differences in degradation behavior.

To measure the degradation of the polymers in the thin film, previous studies assessed degradation by spin-coating the semiconducting polymer on a glass substrate and soaking in acidic solution or degrading the polymer on a degradable substrate (e.g., cellulose and polyvinyl acetate).[20,21,23] These degradation methods suffer from poor reproducibility and inaccurate measurements as physical delamination in aqueous solution can occur irrespective of degradation and degradation of the substrate does not allow for quantification of polymer degradation. To address these limitations, we developed a new method for better estimation of the degradation timescales of conjugated polymer thin films. Specifically, we spin-coated polymers onto OTS-modified $SiO_2$ wafers using the same processing conditions as those used for device fabrication. Then, we used a cured PDMS stamp to peel off the polymer film and placed the film on PDMS facing down into an acidic aqueous solution of 0.5 M TFA (Figure 6a). PDMS was chosen, as it is optically transparent and does not swell in


https://doi.org/10.1021/jacs.1c12845
J. Am. Chem. Soc. XXXX, XXX, XXX−XXX

water, allowing for UV−vis measurements over the degradation timescale of the semiconducting polymer. Additionally, the adhesivity of PDMS ensured that the polymer film did not delaminate for precise measurements as the polymer degraded. To accelerate degradation, we heated these samples in degradation solution at 70 °C.

Using this newly developed floating PDMS protocol, the degradation of the polymer films was quantified in a fashion similar to that shown in Figure 5a, in which the decrease in absorbance at the $\lambda_{max}$ (850 nm for polymer thin films) was plotted over time (Figure 6b,c and Figure S34). In the thin film, the same observations that were seen by solution degradation were followed with a few exceptions. While the effect of branching position and hydrophilicity similarly increased the degradation rate as observed by C1, C4E, and 10TEG polymers relative to C4, $M_n$ had less of an influence in the thin film. Unlike in solution, C8 spacer polymers as well as the 50C8 terpolymer degraded faster than C4, which is correlated more with their decreased $\pi-\pi$ stacking order seen by GIXD. Additionally, hydrophilicity of the sidechains enabled better water diffusion of the degradation solution into the hydrophobic polymer films, as the $\lambda_{max}$ of C4E reached 11% of its initial intensity after 12 weeks compared to 31% for the unfunctionalized C4 sidechain (Figure S35). To ascertain the effect of hydrophilicity, contact angle measurements were conducted, which showed that the C4E polymer film was indeed more hydrophilic than all other polymers (Figure S36 and Table S4). Additionally, despite modest variation in thicknesses of the polymer films (Table S5), a direct relation between thickness and degradation time was not observed likely due to degradation occurring only on the exposed surface of the hydrophobic film. The degradation results both in solution and thin film along with electronic performance are summarized in Table 3. Notably, the trend observed in the degradation rate was almost analogous to the opposite of their trend in electronic performance, as the polymers with the highest mobilities degraded the slowest. This observation suggests similar parameters that dictate electronic performance for semicrystalline polymer semiconductors (e.g., $\pi-\pi$ stacking distance, crystallite size, and degree of crystallinity) also influence degradation of the thin films used to make these transient devices. In addition to aggregation and packing in the thin film, other parameters (e.g., water traps for device performance and hydrophilicity for imine hydrolysis) for the design of degradable semiconductors must be considered.

**Table 3. Summary of Degradation Timescales and Electronic Performance**

| | solution[a] | thin film | |
|---|---|---|---|
| sidechain | time to degradation[b] | time to 50% degradation[c] | $\mu_{sat}$ ($cm^2/V{\cdot}s$) |
| C1 | 14 days | 21 days | 0.32 ± 0.05 |
| C4 | 21 days | 56 days | 0.65 ± 0.16 |
| C8 | 21 days | 21 days | 0.56 ± 0.04 |
| C8L | 21 days | 28 days | 0.42 ± 0.07 |
| C4E | 10 days | 3 days | 0.13 ± 0.01 |
| 10TEG | 14 days | 21 days | 0.46 ± 0.02 |
| 10C8 | 21 days | 42 days | 0.69 ± 0.10 |
| 50C8 | 21 days | 28 days | 0.57 ± 0.01 |

[a]Solution degradation was conducted in chloroform with a 1000-fold molar excess of TFA and water. [b]We defined polymers as degraded when their absorbance intensity at $\lambda_{max}$ was ≤0.05 a.u. [c]Time to 50% degradation is displayed as none of the polymer films reached full degradation as defined in the timescale of the study.

## 3. CONCLUSIONS

In summary, we conducted a systematic study of the influence of molecular design parameters on the lifetime of degradable imine-based semiconducting polymers for transient electronics. In this work, we introduced a series of polymers based on a pDPP-TIT backbone and examined the effect of sidechain branching point, molecular weight, hydrophilicity, and terpolymerization. We demonstrated that both differences in aggregation based on the branching point and $M_n$ as well as the hydrophilicity of the polymers influenced the degradation timescales in solution. Additionally, the solvent that was used had a dramatic impact on their aggregation-dependent degradation. By developing a new method for the study of the polymers' degradation in the thin film, we were able to compare and quantify the degradation of semiconductor films, which showed that many of the parameters we consider for designing high-performance FETs should also be considered for the design of transient electronics. Our results suggest that the incorporation of a small fraction of hydrophilic sidechains through terpolymerization is a potentially promising molecular design approach that results in faster degradation of imine-based polymer semiconductors, while maintaining good charge transport. This study lays the groundwork for establishing molecular design rules for degradable polymer semiconductors, enabling the future advancement of next-generation transient semiconductors with controlled lifetimes.

## ■ ASSOCIATED CONTENT

### Supporting Information

The Supporting Information is available free of charge at https://pubs.acs.org/doi/10.1021/jacs.1c12845.

Detailed synthetic procedure, NMR, additional UV−vis spectra, PESA, AFM, GIXD line profiles, additional FET transfer and output curves, and additional UV−vis degradation data (PDF)

## ■ AUTHOR INFORMATION


### Corresponding Author

**Zhenan Bao** − *Department of Chemistry and Department of Chemical Engineering, Stanford University, Stanford, California 94305, United States;* orcid.org/0000-0002-0972-1715; Email: zbao@stanford.edu

### Authors

**Jerika A. Chiong** − *Department of Chemistry and Department of Chemical Engineering, Stanford University, Stanford, California 94305, United States;* orcid.org/0000-0002-6685-2519

**Yu Zheng** − *Department of Chemistry and Department of Chemical Engineering, Stanford University, Stanford, California 94305, United States;* orcid.org/0000-0001-9854-7378

**Song Zhang** − *Department of Chemical Engineering, Stanford University, Stanford, California 94305, United States*

**Guorong Ma** − *School of Polymer Science and Engineering, The University of Southern Mississippi, Hattiesburg, Mississippi 39406, United States*




https://doi.org/10.1021/jacs.1c12845
J. Am. Chem. Soc. XXXX, XXX, XXX−XXX

**Yilei Wu** − *Department of Chemical Engineering, Stanford University, Stanford, California 94305, United States;* orcid.org/0000-0001-6756-1855

**Gradie Ngaruka** − *Department of Chemical Engineering, Stanford University, Stanford, California 94305, United States*

**Yangju Lin** − *Department of Chemical Engineering, Stanford University, Stanford, California 94305, United States;* orcid.org/0000-0001-6378-7179

**Xiaodan Gu** − *School of Polymer Science and Engineering, The University of Southern Mississippi, Hattiesburg, Mississippi 39406, United States;* orcid.org/0000-0002-1123-3673

Complete contact information is available at: https://pubs.acs.org/10.1021/jacs.1c12845

## Notes

The authors declare no competing financial interest.

## ■ ACKNOWLEDGMENTS

J.A.C. was supported by the National Science Foundation Graduate Research Fellowship under Grant No. DGE-1656518, the Department of Defense (DoD) through the National Defense Science & Engineering Graduate (NDSEG) Fellowship Program, and the Stanford Enhancing Diversity in Graduate Education Doctoral Fellowship Program. G.M. and X.G. thank the financial aid from NSF CHM-2004133 for supporting the scattering portion of this work. Part of this work was performed at the Stanford Nano Shared Facilities (SNSF), supported by the National Science Foundation under award ECCS-1542152. We would like to thank Shayla Nikzad and Nathaniel J. Schuster for helpful advice and discussions.

## ■ REFERENCES

(1) Kang, S.-K.; Yin, L.; Bettinger, C. The Emergence of Transient Electronic Devices. *MRS Bull.* **2020**, *45*, 87−95.

(2) Fu, K. K.; Wang, Z.; Dai, J.; Carter, M.; Hu, L. Transient Electronics: Materials and Devices. *Chem. Mater.* **2016**, *28*, 3527−3539.

(3) Chiong, J. A.; Tran, H.; Lin, Y.; Zheng, Y.; Bao, Z. Integrating Emerging Polymer Chemistries for the Advancement of Recyclable, Biodegradable, and Biocompatible Electronics. *Adv. Sci.* **2021**, *8*, No. 2101233.

(4) Tan, M. J.; Owh, C.; Chee, P. L.; Kyaw, A. K. K.; Kai, D.; Loh, X. J. Biodegradable Electronics: Cornerstone for Sustainable Electronics and Transient Applications. *J. Mater. Chem. C* **2016**, *4*, 5531−5558.

(5) Chen, G.; Xu, L.; Zhang, P.; Chen, B.; Wang, G.; Ji, J.; Pu, X.; Wang, Z. L. Seawater Degradable Triboelectric Nanogenerators for Blue Energy. *Adv. Mater. Technol.* **2020**, *5*, No. 2000455.

(6) Hwang, S.-W.; Tao, H.; Kim, D.-H.; Cheng, H.; Song, J.-K.; Rill, E.; Brenckle, M. A.; Panilaitis, B.; Won, S. M.; Kim, Y.-S.; Song, Y. M.; Yu, K. J.; Ameen, A.; Li, R.; Su, Y.; Yang, M.; Kaplan, D. L.; Zakin, M. R.; Slepian, M. J.; Huang, Y.; Omenetto, F. G.; Rogers, J. A. A Physically Transient Form of Silicon Electronics. *Science* **2012**, *337*, 1640−1644.

(7) Gao, Y.; Zhang, Y.; Wang, X.; Sim, K.; Liu, J.; Chen, J.; Feng, X.; Xu, H.; Yu, C. Moisture-Triggered Physically Transient Electronics. *Sci. Adv.* **2017**, *3*, No. e1701222.

(8) Lee, J.; Yoo, B.; Lee, H.; Cha, G. D.; Lee, H.-S.; Cho, Y.; Kim, S. Y.; Seo, H.; Lee, W.; Son, D.; Kang, M.; Kim, H. M.; Park, Y. I.; Hyeon, T.; Kim, D.-H. Ultra-Wideband Multi-Dye-Sensitized Upconverting Nanoparticles for Information Security Application. *Adv. Mater.* **2017**, *29*, No. 1603169.

(9) Gumus, A.; Alam, A.; Hussain, A. M.; Mishra, K.; Wicaksono, I.; Torres Sevilla, G. A.; Shaikh, S. F.; Diaz, M.; Velling, S.; Ghoneim, M. T.; Ahmed, S. M.; Hussain, M. M. Expandable Polymer Enabled Wirelessly Destructible High-Performance Solid State Electronics. *Adv. Mater. Technol.* **2017**, *2*, No. 1600264.

(10) Boutry, C. M.; Beker, L.; Kaizawa, Y.; Vassos, C.; Tran, H.; Hinckley, A. C.; Pfattner, R.; Niu, S.; Li, J.; Claverie, J.; Wang, Z.; Chang, J.; Fox, P. M.; Bao, Z. Biodegradable and Flexible Arterial-Pulse Sensor for the Wireless Monitoring of Blood Flow. *Nat. Biomed. Eng.* **2019**, *3*, 47−57.

(11) Zheng, Q.; Zou, Y.; Zhang, Y.; Liu, Z.; Shi, B.; Wang, X.; Jin, Y.; Ouyang, H.; Li, Z.; Wang, Z. L. Biodegradable Triboelectric Nanogenerator as a Life-Time Designed Implantable Power Source. *Sci. Adv.* **2016**, *2*, No. e1501478.

(12) Bokka, N.; Selamneni, V.; Sahatiya, P. A Water Destructible SnS 2 QD/PVA Film Based Transient Multifunctional Sensor and Machine Learning Assisted Stimulus Identification for Non-Invasive Personal Care Diagnostics. *Mater. Adv.* **2020**, *1*, 2818−2830.

(13) Feig, V. R.; Tran, H.; Bao, Z. Biodegradable Polymeric Materials in Degradable Electronic Devices. *ACS Cent. Sci.* **2018**, *4*, 337−348.

(14) Tran, H.; Feig, V. R.; Liu, K.; Zheng, Y.; Bao, Z. Polymer Chemistries Underpinning Materials for Skin-Inspired Electronics. *Macromolecules* **2019**, *52*, 3965−3974.

(15) Xu, J.; Wang, S.; Wang, G.-J. N.; Zhu, C.; Luo, S.; Jin, L.; Gu, X.; Chen, S.; Feig, V. R.; To, J. W. F.; Rondeau-Gagné, S.; Park, J.; Schroeder, B. C.; Lu, C.; Oh, J. Y.; Wang, Y.; Kim, Y.-H.; Yan, H.; Sinclair, R.; Zhou, D.; Xue, G.; Murmann, B.; Linder, C.; Cai, W.; Tok, J. B.-H.; Chung, J. W.; Bao, Z. Highly Stretchable Polymer Semiconductor Films through the Nanoconfinement Effect. *Science* **2017**, *355*, 59−64.

(16) Mun, J.; Ochiai, Y.; Wang, W.; Zheng, Y.; Zheng, Y.-Q.; Wu, H.-C.; Matsuhisa, N.; Higashihara, T.; Tok, J. B.-H.; Yun, Y.; Bao, Z. A Design Strategy for High Mobility Stretchable Polymer Semiconductors. *Nat. Commun.* **2021**, *12*, 3572.

(17) Park, S.; Fukuda, K.; Wang, M.; Lee, C.; Yokota, T.; Jin, H.; Jinno, H.; Kimura, H.; Zalar, P.; Matsuhisa, N.; Umezu, S.; Bazan, G. C.; Someya, T. Ultraflexible Near-Infrared Organic Photodetectors for Conformal Photoplethysmogram Sensors. *Adv. Mater.* **2018**, *30*, No. 1802359.

(18) Kim, S.-M.; Jeon, H.; Shin, S.-H.; Park, S.-A.; Jegal, J.; Hwang, S. Y.; Oh, D. X.; Park, J. Superior Toughness and Fast Self-Healing at Room Temperature Engineered by Transparent Elastomers. *Adv. Mater.* **2018**, *30*, No. 1705145.

(19) Harito, C.; Utari, L.; Putra, B. R.; Yuliarto, B.; Purwanto, S.; Zaidi, S. Z. J.; Bavykin, D. V.; Marken, F.; Walsh, F. C. Review—The Development of Wearable Polymer-Based Sensors: Perspectives. *J. Electrochem. Soc.* **2020**, *167*, No. 037566.

(20) Lei, T.; Guan, M.; Liu, J.; Lin, H.-C.; Pfattner, R.; Shaw, L.; McGuire, A. F.; Huang, T.-C.; Shao, L.; Cheng, K.-T.; Tok, J. B.-H.; Bao, Z. Biocompatible and Totally Disintegrable Semiconducting Polymer for Ultrathin and Ultralightweight Transient Electronics. *PNAS* **2017**, *114*, 5107−5112.

(21) Tran, H.; Feig, V. R.; Liu, K.; Wu, H.-C.; Chen, R.; Xu, J.; Deisseroth, K.; Bao, Z. Stretchable and Fully Degradable Semiconductors for Transient Electronics. *ACS Cent. Sci.* **2019**, *5*, 1884−1891.

(22) Tran, H.; Nikzad, S.; Chiong, J. A.; Schuster, N. J.; Peña-Alcántara, A. E.; Feig, V. R.; Zheng, Y.-Q.; Bao, Z. Modular Synthesis of Fully Degradable Imine-Based Semiconducting *p*-Type and *n*-Type Polymers. *Chem. Mater.* **2021**, *33*, 7465−7474.

(23) Park, H.; Kim, Y.; Kim, D.; Lee, S.; Kim, F. S.; Kim, B. J. Disintegrable *n*-Type Electroactive Terpolymers for High-Performance, Transient Organic Electronics. *Adv. Funct. Mater.* **2022**, *32*, No. 2106977.

(24) Sugiyama, F.; Kleinschmidt, A. T.; Kayser, L. V.; Alkhadra, M. A.; Wan, J. M.-H.; Chiang, A. S.-C.; Rodriquez, D.; Root, S. E.; Savagatrup, S.; Lipomi, D. J. Stretchable and Degradable Semiconducting Block Copolymers. *Macromolecules* **2018**, *51*, 5944−5949.

(25) Kamaly, N.; Yameen, B.; Wu, J.; Farokhzad, O. C. Degradable Controlled-Release Polymers and Polymeric Nanoparticles: Mecha-

nisms of Controlling Drug Release. *Chem. Rev.* **2016**, *116*, 2602−2663.
(26) Boehnke, N.; Cam, C.; Bat, E.; Segura, T.; Maynard, H. D. Imine Hydrogels with Tunable Degradability for Tissue Engineering. *Biomacromolecules* **2015**, *16*, 2101−2108.
(27) Sims, M. B.; Patel, K. Y.; Bhatta, M.; Mukherjee, S.; Sumerlin, B. S. Harnessing Imine Diversity To Tune Hyperbranched Polymer Degradation. *Macromolecules* **2018**, *51*, 356−363.
(28) Fukuda, K.; Shimoda, M.; Sukegawa, M.; Nobori, T.; Lehn, J.-M. Doubly Degradable Dynamers: Dynamic Covalent Polymers Based on Reversible Imine Connections and Biodegradable Polyester Units. *Green Chem.* **2012**, *14*, 2907.
(29) Hu, Z.; Haws, R. T.; Fei, Z.; Boufflet, P.; Heeney, M.; Rossky, P. J.; Bout, D. A. V. Impact of Backbone Fluorination on Nanoscale Morphology and Excitonic Coupling in Polythiophenes. *PNAS* **2017**, *114*, 5113−5118.
(30) Zheng, Y.-Q.; Lei, T.; Dou, J.-H.; Xia, X.; Wang, J.-Y.; Liu, C.-J.; Pei, J. Strong Electron-Deficient Polymers Lead to High Electron Mobility in Air and Their Morphology-Dependent Transport Behaviors. *Adv. Mater.* **2016**, *28*, 7213−7219.
(31) Mei, J.; Kim, D. H.; Ayzner, A. L.; Toney, M. F.; Bao, Z. Siloxane-Terminated Solubilizing Side Chains: Bringing Conjugated Polymer Backbones Closer and Boosting Hole Mobilities in Thin-Film Transistors. *J. Am. Chem. Soc.* **2011**, *133*, 20130−20133.
(32) Lei, T.; Dou, J.-H.; Pei, J. Influence of Alkyl Chain Branching Positions on the Hole Mobilities of Polymer Thin-Film Transistors. *Adv. Mater.* **2012**, *24*, 6457−6461.
(33) Kang, I.; Yun, H.-J.; Chung, D. S.; Kwon, S.-K.; Kim, Y.-H. Record High Hole Mobility in Polymer Semiconductors via Side-Chain Engineering. *J. Am. Chem. Soc.* **2013**, *135*, 14896−14899.
(34) Lee, J.; Han, A.-R.; Yu, H.; Shin, T. J.; Yang, C.; Oh, J. H. Boosting the Ambipolar Performance of Solution-Processable Polymer Semiconductors via Hybrid Side-Chain Engineering. *J. Am. Chem. Soc.* **2013**, *135*, 9540−9547.
(35) Raithel, D.; Simine, L.; Pickel, S.; Schötz, K.; Panzer, F.; Baderschneider, S.; Schiefer, D.; Lohwasser, R.; Köhler, J.; Thelakkat, M.; Sommer, M.; Köhler, A.; Rossky, P. J.; Hildner, R. Direct Observation of Backbone Planarization via Side-Chain Alignment in Single Bulky-Substituted Polythiophenes. *PNAS* **2018**, *115*, 2699−2704.
(36) Kang, B.; Kim, R.; Lee, S. B.; Kwon, S.-K.; Kim, Y.-H.; Cho, K. Side-Chain-Induced Rigid Backbone Organization of Polymer Semiconductors through Semifluoroalkyl Side Chains. *J. Am. Chem. Soc.* **2016**, *138*, 3679−3686.
(37) Wu, Y.; Schneider, S.; Walter, C.; Chowdhury, A. H.; Bahrami, B.; Wu, H.-C.; Qiao, Q.; Toney, M. F.; Bao, Z. Fine-Tuning Semiconducting Polymer Self-Aggregation and Crystallinity Enables Optimal Morphology and High-Performance Printed All-Polymer Solar Cells. *J. Am. Chem. Soc.* **2020**, *142*, 392−406.
(38) Meng, B.; Liu, J.; Wang, L. Oligo(Ethylene Glycol) as Side Chains of Conjugated Polymers for Optoelectronic Applications. *Polym. Chem.* **2020**, *11*, 1261−1270.
(39) Wang, N.; Xie, L.; Ling, H.; Piradi, V.; Li, L.; Wang, X.; Zhu, X.; Yan, F. Ethylenedioxythiophene Incorporated Diketopyrrolopyrrole Conjugated Polymers for High-Performance Organic Electrochemical Transistors. *J. Mater. Chem. C* **2021**, *9*, 4260−4266.
(40) Wang, G.-J. N.; Molina-Lopez, F.; Zhang, H.; Xu, J.; Wu, H.-C.; Lopez, J.; Shaw, L.; Mun, J.; Zhang, Q.; Wang, S.; Ehrlich, A.; Bao, Z. Nonhalogenated Solvent Processable and Printable High-Performance Polymer Semiconductor Enabled by Isomeric Nonconjugated Flexible Linkers. *Macromolecules* **2018**, *51*, 4976−4985.
(41) Back, J. Y.; Yu, H.; Song, I.; Kang, I.; Ahn, H.; Shin, T. J.; Kwon, S.-K.; Oh, J. H.; Kim, Y.-H. Investigation of Structure−Property Relationships in Diketopyrrolopyrrole-Based Polymer Semiconductors via Side-Chain Engineering. *Chem. Mater.* **2015**, *27*, 1732−1739.
(42) Kanimozhi, C.; Yaacobi-Gross, N.; Burnett, E. K.; Briseno, A. L.; Anthopoulos, T. D.; Salzner, U.; Patil, S. Use of Side-Chain for Rational Design of *n*-Type Diketopyrrolopyrrole-Based Conjugated Polymers: What Did We Find Out? *Phys. Chem. Chem. Phys.* **2014**, *16*, 17253−17265.
(43) Liu, D.; Mun, J.; Chen, G.; Schuster, N. J.; Wang, W.; Zheng, Y.; Nikzad, S.; Lai, J.-C.; Wu, Y.; Zhong, D.; Lin, Y.; Lei, Y.; Chen, Y.; Gam, S.; Chung, J. W.; Yun, Y.; Tok, J. B.-H.; Bao, Z. A Design Strategy for Intrinsically Stretchable High-Performance Polymer Semiconductors: Incorporating Conjugated Rigid Fused-Rings with Bulky Side Groups. *J. Am. Chem. Soc.* **2021**, *143*, 11679−11689.
(44) Wood, S.; Wade, J.; Shahid, M.; Collado-Fregoso, E.; Bradley, D. D. C.; Durrant, J. R.; Heeney, M.; Kim, J.-S. Natures of Optical Absorption Transitions and Excitation Energy Dependent Photostability of Diketopyrrolopyrrole (DPP)-Based Photovoltaic Copolymers. *Energy Environ. Sci.* **2015**, *8*, 3222−3232.
(45) Sarkar, T.; Schneider, S. A.; Ankonina, G.; Hendsbee, A. D.; Li, Y.; Toney, M. F.; Frey, G. L. Tuning Intra and Intermolecular Interactions for Balanced Hole and Electron Transport in Semiconducting Polymers. *Chem. Mater.* **2020**, *32*, 7338−7346.
(46) Mei, J.; Bao, Z. Side Chain Engineering in Solution-Processable Conjugated Polymers. *Chem. Mater.* **2014**, *26*, 604−615.
(47) Chloroform Solvent Properties. https://macro.lsu.edu/howto/solvents/chloroform.htm (accessed October 13, 2021).
(48) Toluene Solvent Properties. https://macro.lsu.edu/howto/solvents/toluene.htm (accessed October 13, 2021).
(49) Chlorobenzene Solvent Properties. https://macro.lsu.edu/HowTo/solvents/chlorobenzene.htm (accessed October 13, 2021).
(50) Neely, B. J.; Wagner, J.; Robinson, R. L.; Gasem, K. A. M. Mutual Solubility Measurements of Hydrocarbon−Water Systems Containing Benzene, Toluene, and 3-Methylpentane. *J. Chem. Eng. Data* **2008**, *53*, 165−174.
(51) Ye, G.; Liu, Y.; Liu, J.; Qiu, X.; Koster, L. J. A.; Chiechi, R. C. Protonic Acid Doping of Low Band-Gap Conjugated Polyions. *Mater. Chem. Front.* **2020**, *4*, 3585−3593.
(52) Poverenov, E.; Zamoshchik, N.; Patra, A.; Ridelman, Y.; Bendikov, M. Unusual Doping of Donor−Acceptor-Type Conjugated Polymers Using Lewis Acids. *J. Am. Chem. Soc.* **2014**, *136*, 5138−5149.
(53) Fares, A.; Naar, N.; Lamouri, S. Synthesis and Characterization of Schottky Diodes from Polyaniline Doped with Trifluoroacetic Acid. *Polym. Sci., Ser. B* **2021**, *63*, 502−513.


https://doi.org/10.1021/jacs.1c12845
J. Am. Chem. Soc. XXXX, XXX, XXX−XXX